Available online at www.sciencedirect.com
SCIENCE DIRECT®
Journal of Sound and Vibration 292 (2006) 899–910
JOURNAL OF SOUND AND VIBRATION
www.elsevier.com/locate/jsvi

Influence of cylinder pressure on the balancing of a rotary compressor

G. Ferraris[a], M.-A. Andrianoely[a], A. Berlioz[b], R. Dufour[a,*]

[a]*Laboratoire de Dynamique des Machines et des Structures, UMR CNRS 5006, INSA de Lyon, Bâtiment Jean d'Alembert, 18, rue des Sciences, 69621 Villeurbanne, France*

[b]*Laboratoire de Génie Mécanique de Toulouse, EA 813, INSA-Mécanique, 135, Av. de Rangueil, 31077 Toulouse Cedex 4, France*

Received 20 October 2004; received in revised form 5 August 2005; accepted 14 September 2005
Available online 13 December 2005

Abstract

The investigation presented concerns the balancing procedure of a rotary refrigerant compressor subjected to fairly well-known eccentric masses and to a cylinder pressure force. Particular attention is paid to the influence of pressure force on the response of the compressor. The cylinder pressure force is expanded in a Fourier series for evaluating the bearing characteristics, establishing the balancing and predicting the response of the entire compressor. Rotor dynamics, the finite element and influence coefficient methods are used in order to reduce the vibration levels of the rotor and stator parts of the compressor. The prediction focuses in particular on the orbits at the top and bottom of the housing of an industrial compressor. It demonstrates that cylinder pressure plays a negligible role in the case of the rotary machine presented here, but must be taken into account when high pressure and weak bearing characteristics are combined.
© 2005 Elsevier Ltd. All rights reserved.

1. Introduction

The modal method and the influence coefficient method (ICM) are widely used for balancing flexible rotors [1–3] by using a passive approach. The first one uses the modal parameters and modal breakdown of the initial unbalance distribution, the rotor being balanced at its critical speeds, step by step, mode after mode [4]. This method is mostly used for balancing high-speed machinery with critical speeds. The second consists in evaluating the influence of trial masses on the orbits of the planes to be balanced. The solution of the associated inverse problem gives the correction mass combination that minimizes the vibration levels of the target planes (or probes) [2,5]. The balancing speeds of the ICM can be either critical speeds, or any other speeds. The unified approach combines the advantages of the two previous methods [6], i.e. the balancing is also carried out mode after mode but new trial mass sets are determined in such a way that they have no influence on the lowest modes already balanced. In Ref. [7] Kang et al. applied an extension of the unified method to an unsymmetrical rotor–bearing system. Moreover, in Ref. [8] Kang et al. focused on the balancing of a crankshaft for engines. They claim that their proposed approach provides better balancing accuracy than

*Corresponding author. Tel.: +33 4 72 43 82 02; fax: +33 4 72 43 89 30.
E-mail address: regis.dufour@insa-lyon.fr (R. Dufour).

0022-460X/$ - see front matter © 2005 Elsevier Ltd. All rights reserved.
doi:10.1016/j.jsv.2005.09.026

both conventional ICM with consideration errors for balancing symmetrical rotors and the ICM for balancing asymmetrical rotor without measurement errors.

A review on existing active balancing methods has been carried out by Zhou and Shi [9]. However manufacturing of refrigerant compressors is characterized by mass production on several lines. In such cases, passive balancing methods improve reliability and reduce costs.

In the present paper the proposed passive balancing procedure, based on the ICM, concerns a rotary refrigerant compressor subjected to fairly well-known eccentric masses and to a cylinder pressure force, the main objective being to reduce the vibration levels of the rotor and stator parts, in particular at the top and bottom of the housing where pipes and grommets are connected, respectively. The balancing and predicted responses proposed take into account the unbalance mass and the cylinder pressure. Consequently, the results presented in Ref. [10], where only the unbalance masses were considered, are completed.

Section 2 deals with the description of the rotary compressor tested while Section 3 focuses on the finite element (FE) modelling. Section 4 concerns the experimental identification of the cylinder pressure for expanding it with a Fourier series. Section 5 establishes the formulation of the steady-state unbalance mass and asynchronous responses and presents the balancing procedure based either on unbalance mass only or unbalance mass and cylinder pressure force together. Section 6 presents the effect of cylinder pressure on the balancing and on the housing's response to the compressor tested. The implementation of the predicted correction masses in a prototype compressor permits comparing predicted and measured housing responses. Moreover, in order to exhibit the effect of the pressure force, simulations are performed using modified values of the bearing characteristics and cylinder pressure.

2. Rotary compressor description

Refrigerant rotary compressors are composed of rotating (rotor) and non-rotating (stator) parts, see Fig. 1a. The rotor is composed of an electrical rotor fitted onto a crankshaft equipped with a rolling piston (see also Fig. 2). The stator contains an electrical stator press-fitted into a hermetic housing, and a two-fluid-film-bearing crankcase containing the pump and welded inside the housing. Grommets, located at the bottom of the housing, ensure the vibration isolation of the machine. The pump is composed of a cylinder, a rolling piston and a vane–spring system that separate the suction and discharge volumes. The moving mechanical

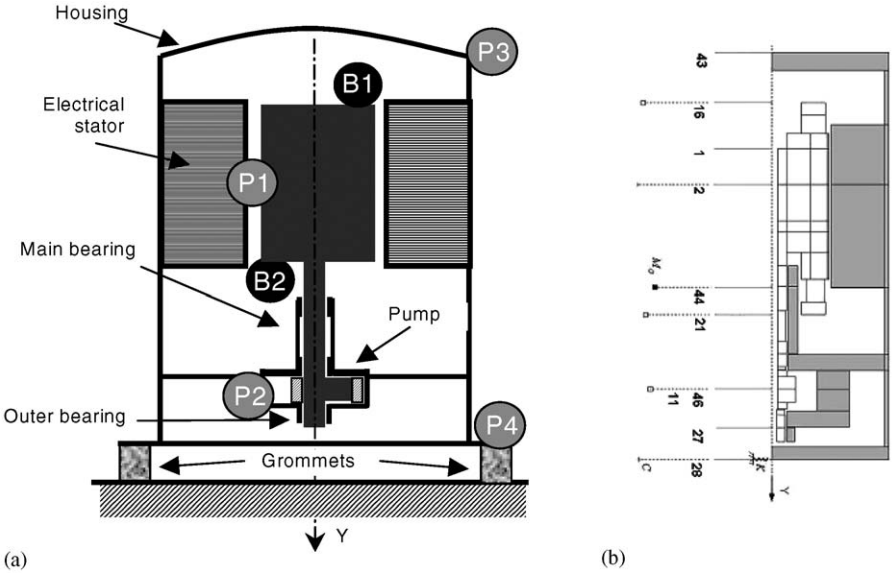

Fig. 1. Sketch (a) and FE model (b) of the rotary compressor.

parts of the pump are lubricated by an oil bath. Imaichi et al. [11] give details on the evaluation of the friction forces.

The rolling piston, crank-pin, and shoulders of the crankshaft have fairly well known eccentric masses. They play a predominant role in the rotor dynamics of the machine relative to the residual unbalance masses due to manufacturing faults and design. In order to provide British Thermal Units (BTU) production adaptable to demand, this compressor is capable of a variable speed of rotation within the (1200–7200 rpm) speed range. Vibrations are transmitted from the rotor to the stator through bearings, fluid, electric fields, etc. Over-pronounced vibration levels occur on the rotor and the stator at certain critical speeds of rotation. This leads to problems such as rotor-to-stator rubs (air gap, fluid film bearings), anchorage failure, energy consumed, noise and vibration transmission through connections and suspension located at the top and bottom of the housing. Therefore, the vibration level of the rotor and stator must be reduced by adequate balancing throughout the speed range.

3. Compressor FE model

The FE model, shown in Fig. 1b, is depicted in detail in Ref. [10] and the rotor dynamics theory presented in Ref. [12]. Each node contains the classical four degrees of freedom (DOF) of the bending motion: two lateral translations and the two associated rotations. The rotor is considered as flexible while the stator is considered as a rigid body mounted on its suspension. The rotor is modelled with two-node beam elements (Nodes 1–27) while the stator is modelled with rigid beam elements with no mass (Nodes from 28 to 44, see the grey parts of Fig. 1b), its mass properties being considered at Node 44, its centre of inertia. The bearings are modelled with one-node bearing elements whose parameters are speed of rotation dependent. Side-pull forces between the electric rotor and the stator are also taken into account. The friction forces between crank-pin and rolling piston, rolling piston and vane, cylinder and vane are assumed to be negligible with respect to the exciting forces. Moreover let the crankshaft run at a speed of rotation Ω, which is assumed to be constant during a cycle. After assembly, the steady-state unbalance response of the compressor is governed by the following matrix equations, see also Ref. [10]:

$$[\mathbf{M}_R + \mathbf{M}_S]\ddot{\mathbf{X}} + [\mathbf{C}(\Omega) + \mathbf{C}_B(\Omega) + \mathbf{C}_G]\dot{\mathbf{X}} + [\mathbf{K}_R + \mathbf{K}_B(\Omega) + \mathbf{K}_{SP} + \mathbf{K}_G]\mathbf{X} = \mathbf{F}(\Omega, n\Omega), \tag{1}$$

with $\mathbf{X}$, the displacement vector containing all the bending DOF of the assembly, $\mathbf{M}_R$ and $\mathbf{K}_R$, the classical mass and stiffness matrices of the rotor; $\mathbf{C}(\Omega)$, the classical non-symmetric gyroscopic matrix; $\mathbf{C}_B(\Omega)$ and $\mathbf{K}_B(\Omega)$, the damping and stiffness matrices due to the bearings; $\mathbf{M}_S$, the mass matrix of the stator; $\mathbf{K}_G$ and $\mathbf{C}_G$, the stiffness and damping matrices associated with the grommets; $\mathbf{K}_{SP}$, the anti-stiffness matrix associated with the side-pull forces, and $\mathbf{F}(\Omega,N\Omega)$, the external force vector expressed by the following combination:

$$\mathbf{F}(\Omega, n\Omega) = \mathbf{F}_{EM}(\Omega) + \mathbf{F}_{CM}(\Omega) + \mathbf{F}_P(\Omega, n\Omega), \tag{2}$$

with $\mathbf{F}_{EM}(\Omega)$, the force vector due to the fairly well-known eccentric masses, $\mathbf{F}_{CM}(\Omega)$, the force vector due to the correction masses, and $\mathbf{F}_p(\Omega, n\Omega)$ the force vector due to the pressure in the cylinder.

4. Experimental set-up and cylinder pressure force identification

The rotary compressor tested was fixed by grommets onto a rigid frame and connected by pipes to an air-conditioning unit. The discharge pressure P_d and suction pressure P_s, see Fig. 2, were measured with transducers connected, respectively, to the cylinder by a short capillary hole and to the inlet pipe. A copper constant thermocouple immersed in the oil bath was used to carry out the experimental investigation under the same temperature conditions. The housing orbits were measured by two perpendicular eddy current sensors see Fig. 3. They were fixed on an adjustable frame and enabled measuring the orbit at the top and bottom of the compressor housing.

Preliminary pressure measurements were carried out versus three different speeds of rotation, i.e. 4860, 6000 and 7200 rpm, see Fig. 4. It was shown that the pressure diagram remains roughly speed of rotation independent. Therefore the approximated pressure diagram plotted in Fig. 5, is available for any speed of rotation involved in the operating range.

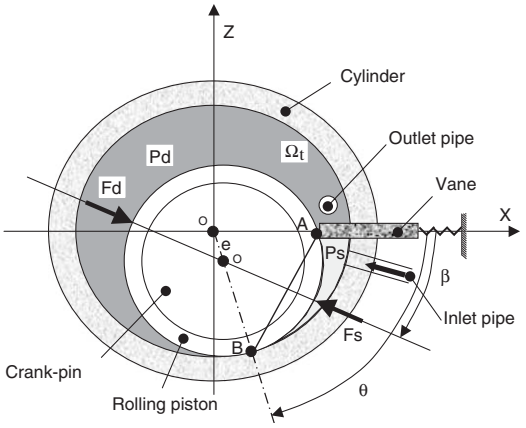

Fig. 2. Suction P_s and discharge P_d pressures in the compressor pump.

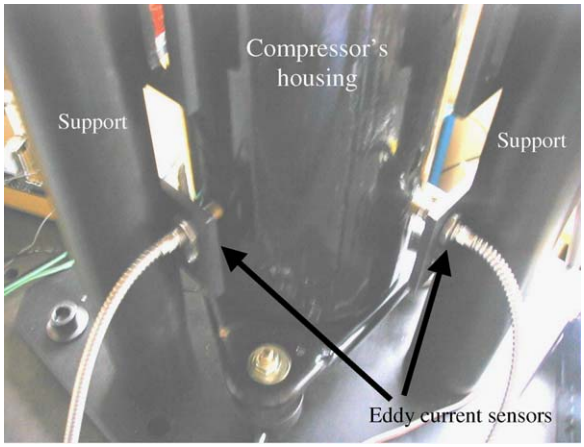

Fig. 3. Compressor equipped with two eddy current sensors.

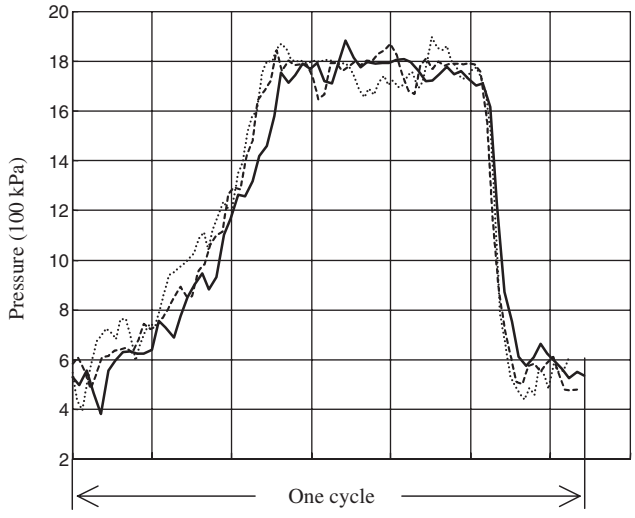

Fig. 4. Measured discharge pressure diagram during one cycle for three speeds of rotation: (···) 4860 rpm, (- - -) 6000 rpm, (—) 7200 rpm.

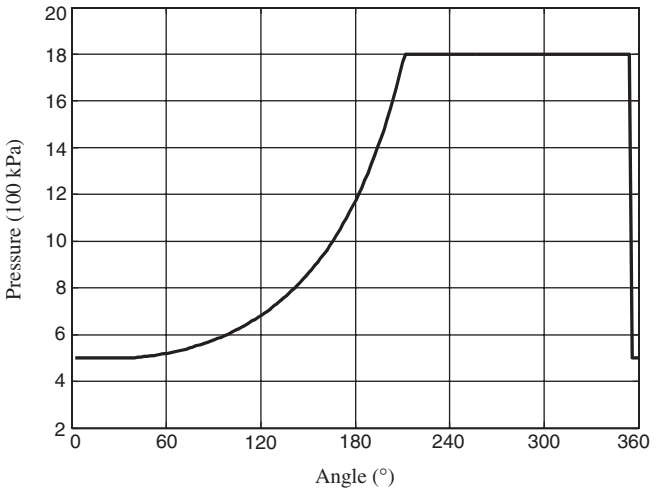

Fig. 5. Curve-fitted pressure diagram.

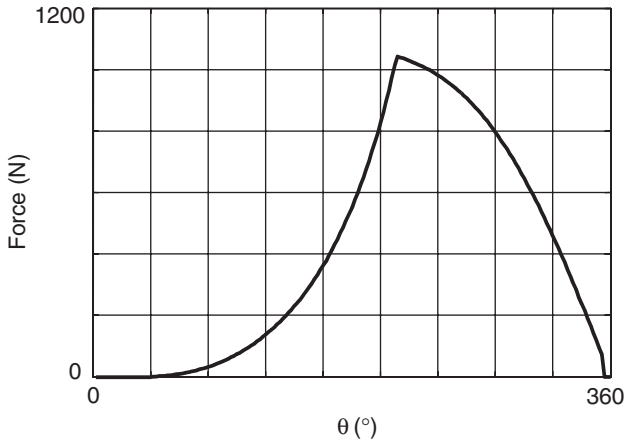

Fig. 6. Pressure force acting on the rolling piston.

The pressure force $\mathbf{F}_P$ acting on the rolling piston, corresponds to the difference between the suction and discharge pressures, see Fig. 6. The amplitude and angular position of force $\mathbf{F}_P$ depend on the angular position of the crankshaft. Therefore the model takes advantage of using Cartesian components $\mathbf{F}_X$,$\mathbf{F}_Z$ along the X- and Z-axis, respectively, see the bold lines of Fig. 7. The $\mathbf{F}_X$,$\mathbf{F}_Z$ components are expanded with four terms using the FFT function of Matlab®, see also Fig. 7. During the steady-state behaviour, each $\mathbf{F}_X$,$\mathbf{F}_Z$ component is expanded in Fourier series and the nth term can be written as

$$F_{Xn} = a_{Xn} \cos n\Omega t + b_{Xn} \sin n\Omega t, \quad F_{Zn} = a_{Zn} \cos n\Omega t + b_{Zn} \sin n\Omega t. \tag{3}$$

Therefore, the pressure force is a summation of synchronous and asynchronous forces. The nth term of the Fourier series is composed of forces that rotate in forward ($\Omega > 0$, subscript f) and backward ($\Omega < 0$, subscript b) directions, respectively,

$$\begin{aligned} F_{Xn} &= f_{fn} \cos(n\Omega t + \varphi_{fn}) + f_{bn} \cos(-n\Omega t + \varphi_{bn}) \\ F_{Zn} &= -f_{fn} \sin(n\Omega t + \varphi_{fn}) - f_{bn} \sin(-n\Omega t + \varphi_{bn}), \end{aligned} \tag{4}$$

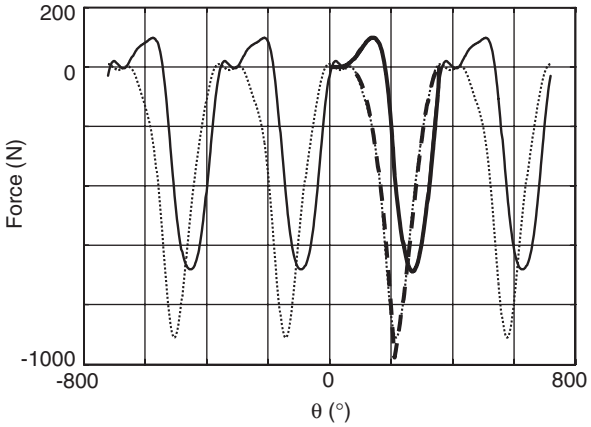

Fig. 7. The pressure force components (bold lines) and their Fourier approximation: (—) $\mathbf{F}_X$, (···) $\mathbf{F}_Z$.

Table 1
Fourier terms for modelling the pressure forces

n	0	1	2	3	4
a_{Xn} (N)	−390.4	−14.7	146.2	7.1	26.6
b_{Xn}(N)		370.9	−31.9	4.3	−2.5
a_{Zn} (N)	−581.5	316.7	−21.1	−11.4	15.8
b_{Zn} (N)		260.5	−144.1	38.8	−22.1
f_{fn} (N)		370.3	147.5	16.3	25.2
φ_{fn} (deg)		−111.8	10.4	167.3	−15.2
f_{bn} (N)		125.9	5.5	24.3	9.4
φ_{bn} (deg)		12.4	−79.5	18.9	−76.2

where $\varphi_{fn}, \varphi_{bn}$ are the phases. Comparing Eqs. (3) and (4) and identifying the sine and cosine terms yield:

$$a_{Xn} = f_{fn}\cos\varphi_{fn} + f_{bn}\cos\varphi_{bn}, \quad b_{Xn} = -f_{fn}\sin\varphi_{fn} + f_{bn}\sin\varphi_{bn},$$
$$a_{Zn} = -f_{fn}\sin\varphi_{fn} - f_{bn}\sin\varphi_{bn}, \quad b_{Zn} = -f_{fn}\cos\varphi_{fn} + f_{bn}\cos\varphi_{bn}. \tag{5}$$

Combining the relationships of Eq. (5) yields the formulation of amplitudes f_{fn}, f_{bn}:

$$f_{fn} = \frac{1}{2}\sqrt{(a_{Xn} - b_{Zn})^2 + (a_{Zn} + b_{Xn})^2}, \quad f_{bn} = \frac{1}{2}\sqrt{(a_{Xn} + b_{Zn})^2 + (b_{Xn} - a_{Zn})^2} \tag{6}$$

and of phases $\varphi_{fn}, \varphi_{bn}$:

$$tg\varphi_{fn} = \frac{\sin\varphi_{fn}}{\cos\varphi_{fn}} = -\frac{a_{Zn} + b_{Xn}}{a_{Xn} - b_{Zn}}, \quad tg\varphi_{bn} = \frac{\sin\varphi_{bn}}{\cos\varphi_{bn}} = \frac{b_{Xn} - a_{Zn}}{a_{Xn} + b_{Zn}}. \tag{7}$$

Table 1 shows the distribution of the first four Fourier coefficients given by Eq. (5), which are in fact the more significant terms, and the amplitudes and phases of the asynchronous forces expressed with Eqs. (6) and (7). The a_{X0} and a_{Z0} coefficients lead to a constant load used for calculating the stiffness and damping coefficients of the fluid film bearings, [13,14]. Here these forces are applied to the crankshaft (Node 11) and their opposite forces on the stator (Node 46).

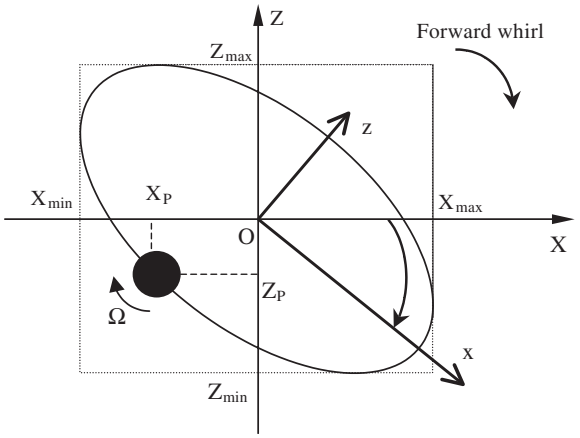

Fig. 8. Ellipse description.

5. Balancing and steady-state unbalance and asynchronous responses

5.1. Orbits

The rotary compressor is subjected to fairly well-known eccentric masses, correction masses and, cylinder pressure force. Here, these types of excitation are superposed in the calculation process. Particular attention is paid to the calculation of the trajectory of any node of the FE model. Let **U** and **W** be the lateral DOF along the *X*- and *Z*-axis, respectively:

$$\mathbf{U} = \mathbf{A}\cos\Omega t + \mathbf{B}\sin\Omega t, \quad \mathbf{W} = \mathbf{C}\cos\Omega t + \mathbf{D}\sin\Omega t, \tag{8}$$

where **A**, **B**, **C** and **D** are constant. Combining **U** with **W** yields an orbit, which is an ellipse, see Fig. 8. The different contributions are, for the eccentric and correction masses:

$$\begin{aligned}\mathbf{U}_{\mathrm{EM+CM}} &= \mathbf{A}_{\mathrm{EM+CM}}\cos\Omega t + \mathbf{B}_{\mathrm{EM+CM}}\sin\Omega t,\\ \mathbf{W}_{\mathrm{EM+CM}} &= \mathbf{C}_{\mathrm{EM+CM}}\cos\Omega t + \mathbf{D}_{\mathrm{EM+CM}}\sin\Omega t\end{aligned} \tag{9}$$

for each Fourier series term of the forward pressure force:

$$\mathbf{U}_{fn} = \mathbf{A}_{fn}\cos\Omega t + \mathbf{B}_{fn}\sin\Omega t, \quad \mathbf{W}_{fn} = \mathbf{C}_{fn}\cos\Omega t + \mathbf{D}_{fn}\sin\Omega t \tag{10}$$

and for each Fourier series term of the backward pressure force:

$$\mathbf{U}_{bn} = \mathbf{A}_{bn}\cos\Omega t + \mathbf{B}_{bn}\sin\Omega t, \quad \mathbf{W}_{bn} = \mathbf{C}_{bn}\cos\Omega t + \mathbf{D}_{bn}\sin\Omega t. \tag{11}$$

Consequently the lateral trajectory, or orbits, of a node is described with $\mathbf{U}_T$, $\mathbf{W}_T$, which are the superposition of displacements (9), and of the N displacements given by Eqs. (10) and (11)

$$\mathbf{U}_T = \mathbf{U}_{\mathrm{EM+CM}} + \sum_{n=1}^{N}(\mathbf{U}_{fn} + \mathbf{U}_{bn}), \quad \mathbf{W}_T = \mathbf{W}_{\mathrm{EM+CM}} + \sum_{n=1}^{N}(\mathbf{W}_{fn} + \mathbf{W}_{bn}). \tag{12}$$

5.2. Balancing procedure

The objective is to minimize the vibration level of the rotating and non-rotating parts of the compressor. First of all, the amplitudes and phases predicted with the FE rotor dynamics software Rotorinsa® developed by Lalanne and Ferraris [12] are the input data of the ICM balancing software Flxbal® developed by Adams [15]. The Sève et al software developed in Ref. [10], integrates both the rotor dynamics software Rotorinsa® and the IC method. The Flxbal® software is required since this integration makes it impossible to incorporate the synchronous pressure force in the balancing.

Table 2
Predicted correction masses with the balancing # 1 (based only on the eccentric masses)

	Computer code	Existing compressor		Modified compressor	
		Mass (g)	Angle (deg)	Mass (g)	Angle (deg)
Correction mass Balancing plane B1 Node 16, radius 15.0 mm	Adams [15]	16.9	4.6	12.2	33.5
	Sève et al. [10]	12.7	−14.8		
Correction mass Balancing plane B2 Node 21, radius 14.5 mm	Adams [15]	74.5	178.2	94.8	172.3
	Sève et al. [10]	96.9	178.3		

Table 3
Predicted correction masses with the balancing #2 (based on the eccentric masses and on synchronous pressure force)

	Computer code	Existing compressor		Modified compressor	
		Mass (g)	Angle (deg)	Mass (g)	Angle (deg)
Correction mass Balancing plane B1 Node 16, radius 15 mm	Adams [15]	16.9	5.1	19.2	16.7
Correction mass Balancing plane B2 Node 21, radius 14.5 mm	Adams [15]	74.5	178.3	108.6	175.2

Balancing #1 is carried out taking into account the eccentric masses of the pump only while balancing #2 is based on the eccentric masses and on the synchronous force, i.e. the order $n = 1$ of the Fourier series of the cylinder pressure force.

Balancing with the IC method is composed of three computation steps. Step #1 predicts the response to the initial eccentric masses, step #2 the response to the initial eccentric masses and to the first trial-mass set, and step #3 the response to the initial eccentric masses and to the second trial-mass set. It should be mentioned that each response, defined by amplitude and phase, is predicted for the balancing speeds of rotation and for the nodes belonging to the target planes (or probes).

This procedure is available for balancing #1, and the correction masses are distributed in Table 2. In the case of balancing #2 the procedure must be completed with the successive calculation of the responses to the forward and backward synchronous forces. Broadly speaking, in each computation step the superposition of several responses must be done as indicated by formula (12) with $n = 1$. In this case the correction masses obtained are catalogued in Table 3.

In the rotary compressor tested, industrial requirements demand that two existing balancing planes be retained: B1 at the top (Node 16) and B2 at the bottom (Node 21) of the electrical rotor, see Fig. 1a. The initial eccentric mass (mass = 162 g, radius = 5.6 mm, phase = 0°) due to the mechanical parts of the pump is located at Node 11 while the target planes are situated on the rotor (P1 at Node 2, P2 at Node 11) and at the top (P3 at Node 43) and bottom (P4 at Node 28) of the stator, as mentioned by Fig. 1a. The balancing performed at 2400 and 7200 rpm provides the mass and the phase of the two correction masses.

In order to magnify the influence of pressure, simulations are also performed on a modified compressor having the same characteristics as previously, except the bearing stiffness and damping divided by ten and the cylinder pressure multiplied by 10.

Analysis of Tables 2 and 3 makes it possible to conclude that the correction masses obtained by the two computer codes are rather close. Moreover those obtained with and without the synchronous cylinder pressure force are very close for the existing compressor: the synchronous pressure force has a negligible influence on its balancing.

6. Housing responses of the existing compressor and of a modified compressor

6.1. Simulation investigation

Only the orbits at the top (Node 43) and bottom (Node 28) of the compressor housing are presented. Four types of unbalance response are predicted at three different speeds of rotations (2400, 4800 and 7200 rpm):

- the response noted EM due to the eccentric masses with no balancing,
- the response noted EM + PR, which is the superposition of the unbalance response due to the eccentric masses and of the $N = 4$ responses due to the cylinder pressure, with no balancing performed,
- the response, noted Bal#1 + PR, based on balancing #1 and on the $N = 4$ responses due to the cylinder pressure, the balancing performed with the computer codes developed by Adams [15] and Sève et al. [10] being based on eccentric mass only, see Table 2.
- the response, noted Bal#2 + PR, based on balancing #2 and on the $N = 4$ responses due to the cylinder pressure.

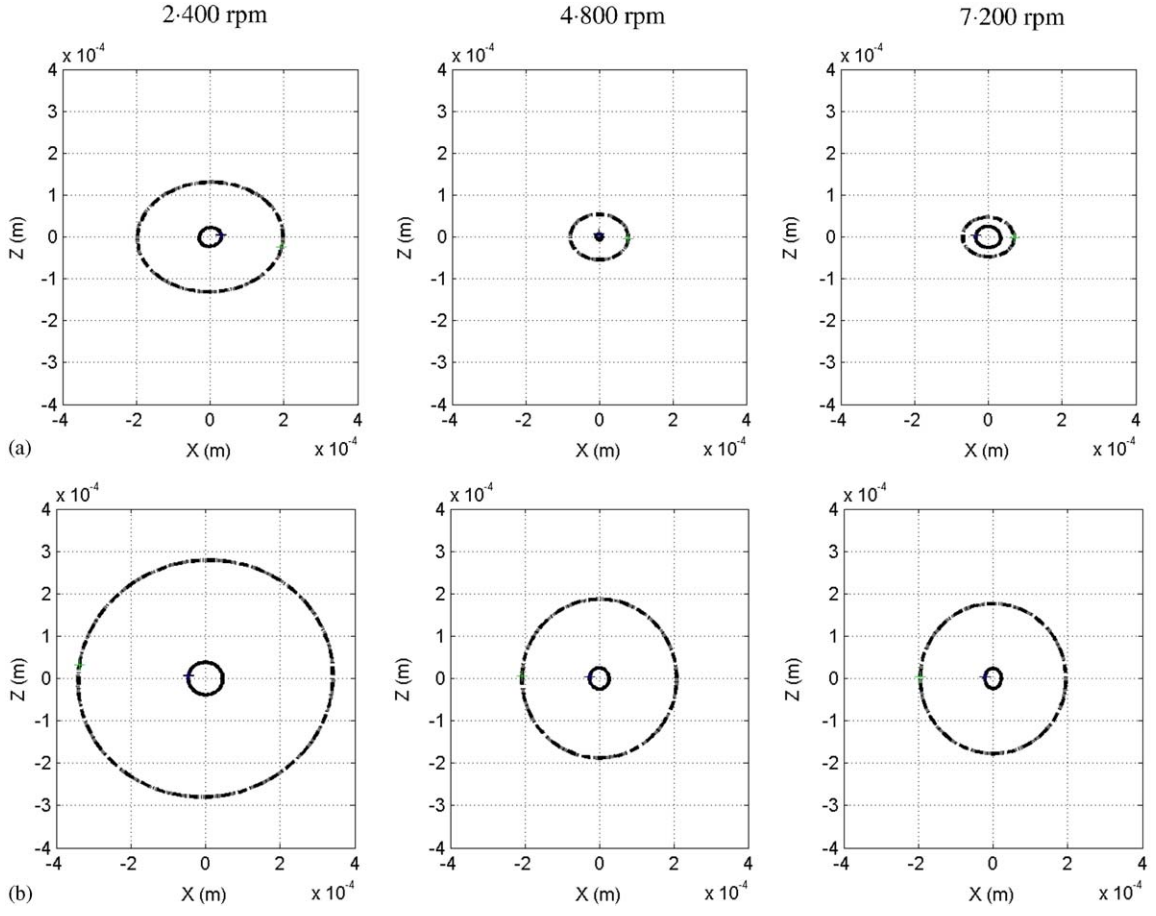

Fig. 9. Orbits at the top (a) and bottom (b) of the existing compressor's housing: (– – –) EM, (– · – · –) EM + PR, (· · · · · · · · ·) Bal #1 + PR, (——) Bal #2 + PR.

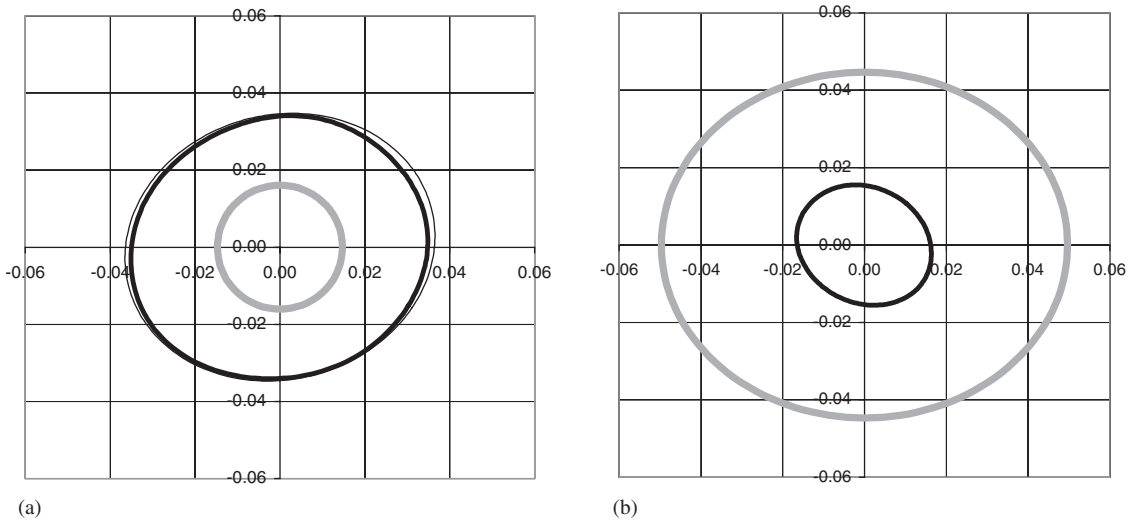

Fig. 10. Existing compressor: measured and predicted orbits at the top (a) and bottom (b) of the housing at 4800 rpm: (—) Bal #1, (▬) Bal #1 + PR, (▬) Experiment.

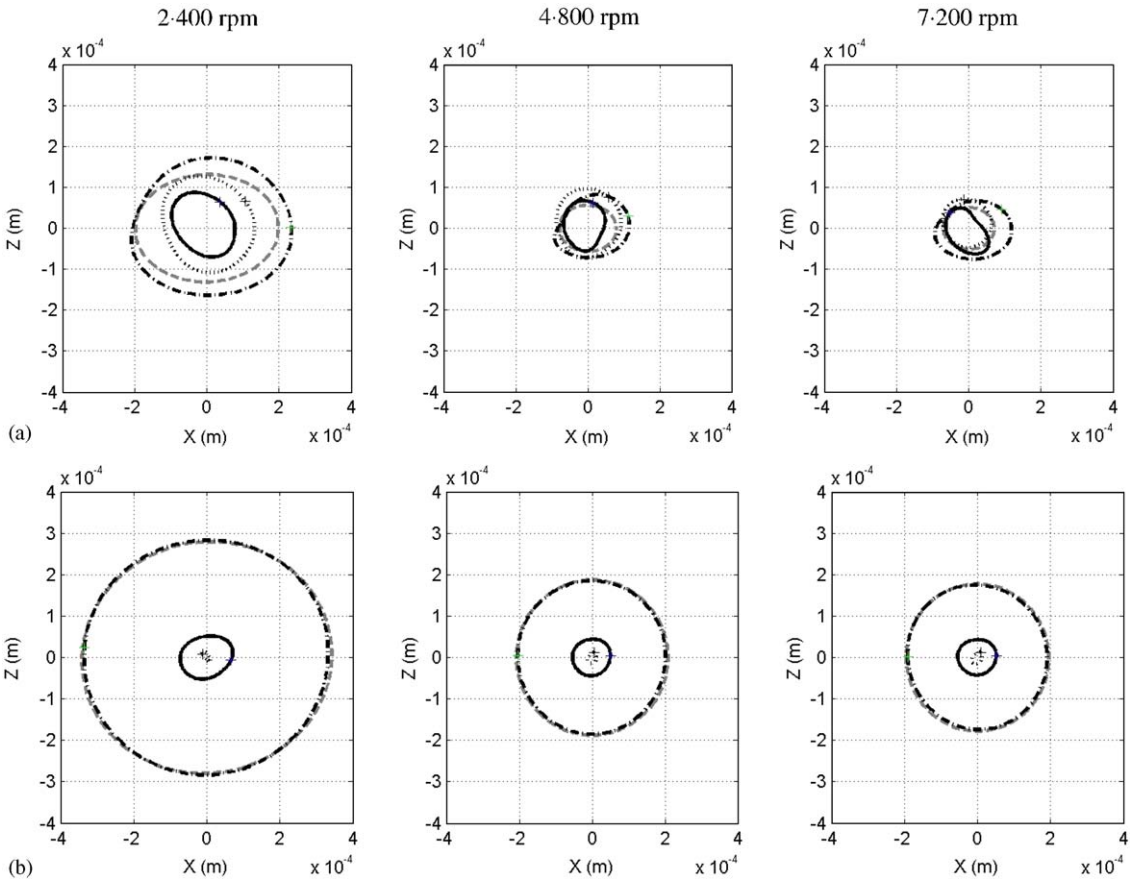

Fig. 11. Modified compressor: orbits at the top (a) and bottom (b) of the housing, keys as Fig. 9.

6.2. Response of the existing compressor

The comparison of the orbits at the top and bottom of the existing compressor housing presented in Fig. 9, shows that unbalance responses EM and EM + PR are similar: pressure plays a negligible role on the unbalance responses. Thus the assumption made in Ref. [10] is verified. A same conclusion can be drawn from balance responses Bal#1 + PR and Bal#2 + PR. The balancing based on the eccentric mass only is very efficient, enough for the existing compressor. The correction masses given by Sève et al. [10], see also Table 2, have been implemented in a compressor prototype. Fig. 10 compares the predicted (with Ref. [10]) and measured responses of the Bal#1 + PR configuration: the presence of pressure does not enhance the predicted response.

6.3. Response of the modified compressor

In the case of the modified compressor, comparison of the orbits at the top and bottom of the housing presented in Fig. 11, shows that unbalance responses EM and EM + PR are slightly different, especially at the top of the housing. It can be stated that the balancing based on eccentric mass is enough. The same conclusion can be drawn for Bal#1 + PR and Bal#2 + PR responses. The balancing based on the eccentric mass only is efficient.

7. Conclusion

The influence of cylinder pressure on the balancing procedure and on the lateral response of the industrial rotary refrigerant compressor tested was investigated numerically and experimentally. The compressor was subjected to fairly well-known eccentric masses and to a cylinder pressure force. As the pressure is expanded in Fourier series, the synchronous part of the expansion was introduced in the balancing procedure in order to quantify its role in the unbalance response.

Using the rotor dynamics theory, the FE method and two balancing computer codes based on the ICM leads to the following conclusion. In the case of the industrial compressor studied here, cylinder pressure plays a negligible role on the balancing procedure and on its response, in comparison of the unbalance force. Consequently the assumption made in a previous paper is verified.

Acknowledgements

The authors are indebted to Tecumseh Europe and to the *Rhône-Alpes* Council for their supports.

References

[1] R.E.D. Bishop, G.M.L. Gladwell, The vibration and balancing of an unbalance flexible rotor, *Journal of Mechanical Engineering for Science* 1 (1959) 66–77.
[2] A.G. Parkinson, The balancing of flexible rotors, *Proceedings of the IUTAM Symposium on Dynamics of Rotors*, Lingby, 1974, pp. 413–435.
[3] J.W. Lund, J. Tonnesen, Analyses and experiments on multi-plane balancing of a flexible rotor, *ASME Journal of Engineering for Industry* 94 (1972) 233–242.
[4] S. Saito, T. Azuma, Balancing of flexible rotors by the complex modal method, *ASME Journal of Mechanical Design* 105 (1981) 94–105.
[5] T.P. Goodman, A least squares method for computing balance correction masses, *ASME Journal of Engineering for Industry* 8 (1964) 273–279.
[6] A.G. Parkinson, M.S. Darlow, A.J. Smalley, A theoretical introduction to the development of a unified approach to flexible rotor balancing, *Journal of Sound and Vibration* 68 (4) (1980) 489–506.
[7] Y. Kang, G.J. Sheen, S.M. Wang, Development and modification of a unified balancing method for unsymmetrical rotor bearing systems, *Journal of Sound and Vibration* 199 (3) (1997) 349–369.
[8] Y. Kang, M.-H. Tseng, S.-M. Wang, C.-P. Chiang, C.-C. Wang, An accuracy improvement for balancing crankshafts, *Mechanism and Machine Theory* 38 (2003) 1449–1467.

[9] S. Zhou, S. Shi, Active balancing and vibration control of rotating machinery: a survey, *The Shock and Vibration Digest* 33 (5) (2001) 361–371.
[10] F. Sève, M.-A. Andrianoely, A. Berlioz, R. Dufour, M. Charreyron, Balancing of machinery with flexible variable speed rotor, *Journal of Sound and Vibration* 264 (2) (2003) 287–302.
[11] K. Imaichi, M. Fukushima, S. Muramatsu, N. Ishii, Vibration analysis of rotary compressors, *Proceedings of the Purdue Compressor Technology Conference*, West Lafayette, IN, 1982, pp. 275–282.
[12] M. Lalanne, G. Ferraris, *Rotordynamics Prediction in Engineering*, second ed., Wiley, New York, 1998.
[13] T. Tsuneo Someya, *Journal-bearing Databook*, Springer, Berlin, 1989.
[14] R. Dufour, M. Gérard, M. Charreyron, Dynamic Analysis of a crankshaft in bending with an electric motor and non-linear fluid bearing, *IFToMM Rotordynamics Conference*, Darmstadt, 1998, pp. 200–211.
[15] L.M. Adams, J.R. Adams, *Rotating Machinery Vibration from Analysis to Troubleshooting*, Marcel Dekker Inc., New York, Basel, 2001.